Tidal evolution of discy dwarf galaxies in the Milky Way potential: the formation of dwarf spheroidals

Klimentowski, J ; Lokas, E L ; Kazantzidis, S ; Mayer, L ; Mamon, G A

Abstract: We conduct high-resolution collisionless N-body simulations to investigate the tidal evolution of dwarf galaxies on an eccentric orbit in the Milky Way (MW) potential. The dwarfs originally consist of a low surface brightness stellar disc embedded in a cosmologically motivated dark matter halo. During 10 Gyr of dynamical evolution and after five pericentre passages, the dwarfs suffer substantial mass loss and their stellar component undergoes a major morphological transformation from a disc to a bar and finally to a spheroid. The bar is preserved for most of the time as the angular momentum is transferred outside the galaxy. A dwarf spheroidal (dSph) galaxy is formed via gradual shortening of the bar. This work thus provides a comprehensive quantitative explanation of a potentially crucial morphological transformation mechanism for dwarf galaxies that operates in groups as well as in clusters. We compare three cases with different initial inclinations of the disc and find that the evolution is fastest when the disc is coplanar with the orbit. Despite the strong tidal perturbations and mass loss, the dwarfs remain dark matter dominated. For most of the time, the one-dimensional stellar velocity dispersion, , follows the maximum circular velocity, Vmax, and they are both good tracers of the bound mass. Specifically, we find that $M_{bound} \propto V_{max}^{3.5} and V_{max} \sim \sqrt{3}\sigma in agreement with earlier studies based on pure dark matter simulations. The latter relation is based on directly measuring$

DOI: https://doi.org/10.1111/j.1365-2966.2009.15046.x

Mon. Not. R. Astron. Soc. **000**, 000–000 (0000) Printed 5 February 2011 (MN LATEX style file v2.2)

Tidal evolution of a disky dwarf galaxy in the Milky Way potential: the formation of a dwarf spheroidal

Jarosław Klimentowski,[1] Ewa L. Łokas,[1] Stelios Kazantzidis,[2,3] Lucio Mayer,[4,5] Gary A. Mamon[6,7] and Francisco Prada[8]

[1] *Nicolaus Copernicus Astronomical Center, Bartycka 18, 00-716 Warsaw, Poland*
[2] *Kavli Institute for Particle Astrophysics and Cosmology, Department of Physics, Stanford University, P.O. Box 20450, M/S 29, Stanford, CA 94309, USA*
[3] *Present Address: Center for Cosmology and Astro-Particle Physics; and Department of Physics; and Department of Astronomy, The Ohio State University, Physics Research Building, 191 West Woodruff Avenue, Columbus, OH 43210, USA*
[4] *Institute for Theoretical Physics, University of Zürich, CH-8057 Zürich, Switzerland*
[5] *Institute of Astronomy, Department of Physics, ETH Zürich, Wolfgang-Pauli Strasse, CH-8093 Zürich, Switzerland*
[6] *Institut d'Astrophysique de Paris (UMR 7095: CNRS and Université Pierre & Marie Curie), 98 bis Bd Arago, F-75014 Paris, France*
[7] *GEPI (UMR 8111: CNRS and Université Denis Diderot), Observatoire de Paris, F-92195 Meudon, France*
[8] *Instituto de Astrofísica de Andalucia (CSIC), Apartado Correos 3005, E-18080 Granada, Spain*

5 February 2011

ABSTRACT

We conduct a high-resolution collisionless N-body simulation to investigate the tidal evolution of a dwarf galaxy on an eccentric orbit in the Milky Way (MW) potential. The dwarf originally consists of a low surface brightness stellar disk embedded in a cosmologically motivated dark matter halo. During 10 Gyr of dynamical evolution and after 5 pericentre passages the dwarf suffers substantial mass loss and its stellar component undergoes a major morphological transformation from a disk to a bar and finally to a spheroid. The bar is preserved for most of the time, as long as angular momentum is transferred outside the galaxy. A dwarf spheroidal (dSph) galaxy is formed only after the last pericentre when the average angular momentum per stellar particle increases. Despite the strong tidal perturbations and mass loss, for most of the time the 1D stellar velocity dispersion, σ, follows the maximum circular velocity, $V_{\rm max}$, and they are both good tracers of the bound mass. Specifically, we find that $M_{\rm bound} \propto V_{\rm max}^{3.5}$ and $V_{\rm max} \sim 2\sigma$. The latter relation is based on directly measuring the stellar kinematics of the simulated dwarf and may thus be used to map the observed stellar velocity dispersions of dSphs to halo circular velocities when formulating the missing satellites problem. We also study the properties of tidal tails formed during the evolution of the dwarf. We report on an interesting phenomenon of 'tidal tail flipping': on the way from the pericentre to the apocentre the old tails following the orbit are dissolved and new ones pointing towards the MW are formed over a short timescale. Contrary to common belief, we find that in the vicinity of the dwarf (where they are most likely to be detectable) the tails are typically oriented towards the MW and not along the orbit. We also find a linear relation between the velocity of stars in the tidal tails and their distance from the dwarf.

Key words: galaxies: Local Group – galaxies: dwarf – galaxies: fundamental parameters – galaxies: kinematics and dynamics – cosmology: dark matter

1 INTRODUCTION

In the currently favoured cold dark matter (CDM) paradigm of hierarchical structure formation, structure develops from the 'bottom-up' as small, dense dark matter clumps collapse first and subsequently undergo a series of mergers that result in the hierarchical formation of large, massive dark matter haloes. According to this model, dwarf galaxies constitute the building blocks of larger galaxies and those that have survived until now are expected to be among the oldest structures in the Universe. Cosmological N-body simulations set within the CDM paradigm predict too many substructures around galaxy-sized systems compared to the

number of dwarf galaxy satellites of the Milky Way (MW) and M31 (Klypin et al. 1999; Moore et al. 1999), giving rise to the so-called 'missing satellites' problem. It is still unclear whether this problem lies in the theory or in the inadequacy of current observations for very faint galaxies (for a review see Kravtsov, Gnedin & Klypin 2004a; Simon & Geha 2007).

Among the dwarf galaxies of the Local Group (see Mateo 1998 for a review), dwarf spheroidals (dSph) are the most numerous. Owing to their proximity to the primary galaxies it is entirely plausible that dSphs have been affected by tidal interactions. Their stellar distribution is supported by velocity dispersion and under the assumption that they are in dynamical equilibrium, dSphs are characterized by very high dark matter contents and mass-to-light ratios. Though it has been suggested that such high velocity dispersions may result from lack of virial equilibrium (Kuhn & Miller 1989) or even non-Newtonian dynamics like MOND (Milgrom 1995; Łokas 2001), the general consensus is that dSphs are the most dark matter dominated galaxies in the Universe (Gilmore et al. 2007).

With increasing accuracy of observational data more precise studies of dSph dynamics can be performed. Recently, their nearly flat velocity dispersion profiles have been modelled using the Jeans formalism assuming a compact stellar component embedded in an extended dark matter halo (Łokas 2002; Kleyna et al. 2002). However, there are still uncertainties concerning the exact form of the dark matter density distribution. For example Walker et al. (2006) exclude that dark matter follows light in the Fornax dSph, while Klimentowski et al. (2007) argue that it is possible to fit a constant mass-to-light ratio if unbound stars are removed from the kinematic sample.

In recent years, two types of numerical studies have been performed to elucidate the origin and evolution of dSphs. The first is based on cosmological N-body simulations that follow only the dark matter component. A region of the size of the Local Group or of a MW-sized halo is selected at $z = 0$, traced back to the initial conditions and then resimulated with higher resolution (Klypin et al. 2001; see also Kravtsov et al. 2004a; Warnick & Knebe 2006; Diemand, Kuhlen & Madau 2007; Martinez-Vaquero, Yepes & Hoffman 2007 for examples of this approach). This strategy allows to accurately study the formation and evolution of host haloes and their substructure. However, because the baryonic component is neglected, it cannot address the internal structure and kinematics of dwarfs.

The second approach is based on evolving a high-resolution numerical model of a single dwarf galaxy placed on a representative orbit around its host. In most cases, the host galaxy is represented by a static external potential (e.g. Johnston, Sigurdsson & Hernquist 1999; Mayer et al. 2001; Hayashi et al. 2003; Kazantzidis, Magorrian & Moore 2004a; Kazantzidis et al. 2004b; Helmi 2004; Klimentowski et al. 2007; Peñarrubia, Navarro & McConnachie 2008). With this method one readily isolates the effects of tidal interactions on the internal structure and kinematics of the dwarf. However, this approach requires making assumptions regarding the initial conditions and neglects the effects of dynamical friction, the evolution of the host galaxy's potential, or interactions between dwarfs.

In this paper we adopt the second approach. Our initial conditions are based on the 'tidal stirring' model (Mayer et al. 2001). In particular, the progenitor dwarf comprises a low surface brightness stellar disk embedded in a dark matter halo, and it is placed on an eccentric orbit within a static potential representing the MW. We aim at elucidating the dynamical mechanisms whereby a disky dwarf can be transformed into a spheroidal galaxy and how the evolution occurs. In addition, we investigate the relation between the stellar velocity dispersion, the maximum circular velocity and the bound mass of the dwarf as a function of

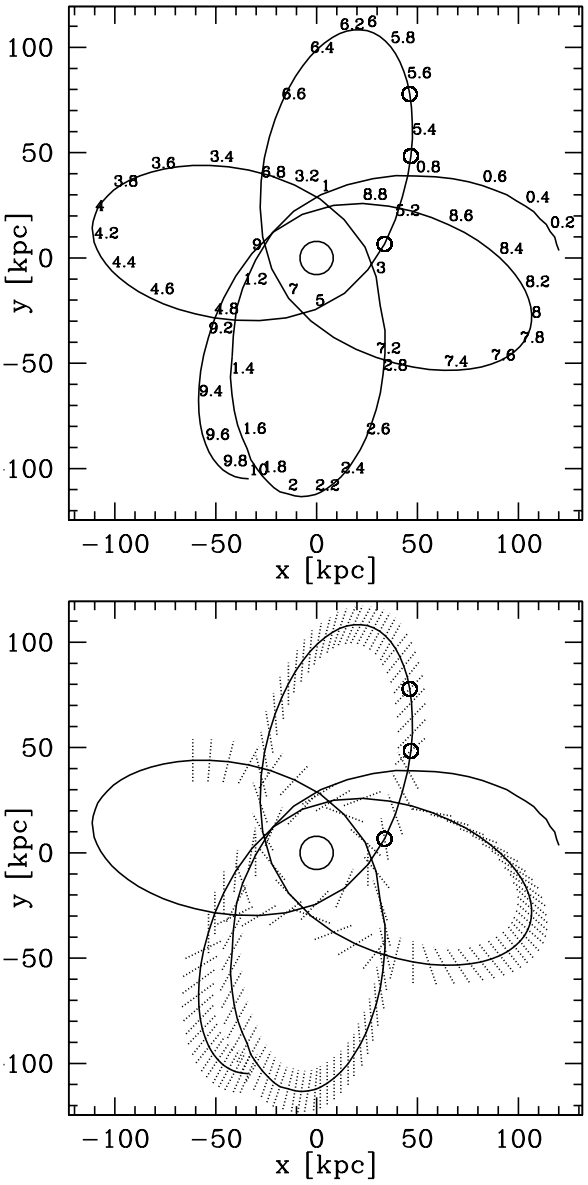

Figure 1. The upper panel shows the whole orbit of the simulated dwarf galaxy projected on the plane of the MW disk. The simulation starts at the right-hand side of the Figure. Numbers indicate the time from the start of the simulation in Gyr. In the lower panel dotted lines overplotted on the orbit show the direction of the tidal tails. In the parts that lack dotted lines no tidal tails were found, i.e. the matter stripped from the dwarf was distributed uniformly around the galaxy. The large circle in the middle of each panel shows the position of the host galaxy. Smaller circles marked on the orbit correspond to the snapshots presented in Fig. 13.

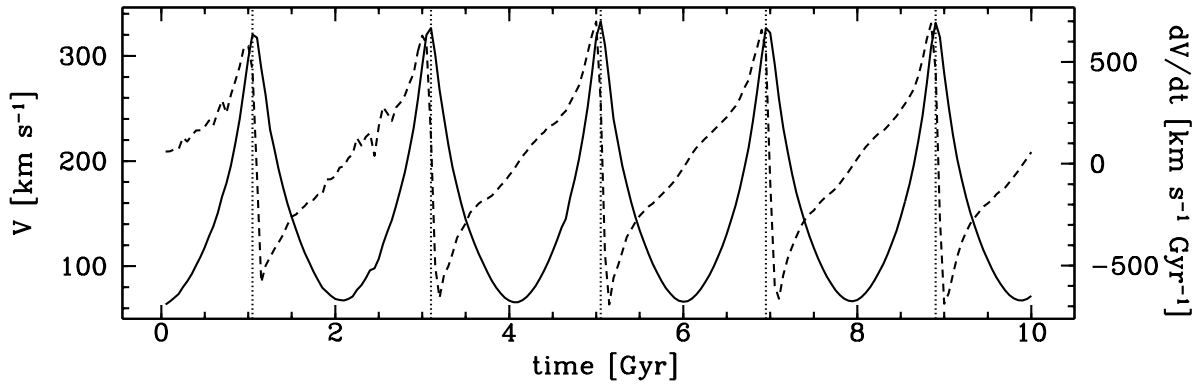

Figure 2. The velocity of the dwarf galaxy (solid line, left axis) and its acceleration (dashed line, right axis) as a function of time. Vertical dotted lines indicate pericentre passages.

time. Knowing these relations is crucial for interpreting correctly the missing satellites problem as they reflect the link between dark halo properties and observable properties of dSphs. Finally, we also study the dynamics of stellar tidal tails produced as the dwarf is stripped by the host potential. The paper is organized as follows. In section 2 we summarize the simulation details. In section 3 we study the galaxy evolution in terms of the mass loss, morphological transformation and changes in internal kinematics. Section 4 is devoted to the description of the tidal tails, their alignment and dynamics. The discussion follows in section 5.

2 THE SIMULATION

In this section we summarize the most important features of the simulation used for this study (see Klimentowski et al. 2007 for details). The simulation was designed according to the 'tidal stirring' scenario proposed by Mayer et al. (2001) which suggests that the progenitors of the majority of dSph galaxies were rotationally supported low surface brightness disky dwarfs similar to present-day dwarf irregulars.

The dwarf progenitor consists of a stellar disk embedded in a dark matter halo. The disk is modelled by $N = 10^6$ particles. Its density drops exponentially with radius in the rotation plane and its vertical structure is modelled by isothermal sheets. The dark matter halo consists of $N = 4 \times 10^6$ particles which are distributed according to the NFW profile. The concentration parameter of the NFW halo is $c = 15$. Beyond the virial radius the profile was cut-off with an exponential function to keep the total mass finite (Kazantzidis et al. 2004a). The total mass of the progenitor was $M = 4 \times 10^9$ $M_\odot$ (the virial mass is $M_{\rm vir} = 3.7 \times 10^9$ $M_\odot$) which corresponds to the virial velocity of 20 km s^{-1}. The models include adiabatic contraction of the halo in response to the baryons. The peak velocity $V_{\rm max}$ is initially equal to 30 km s^{-1}.

The dwarf galaxy evolves on its orbit around the host galaxy which is modelled by a static gravitational potential. This approach neglects several effects like dynamical friction or evolution of the host galaxy itself. However, for our setup the timescale of the dynamical friction should significantly exceed the orbital timescale (Colpi, Mayer & Governato 1999), while the host halo should be already in place by the time the dwarf enters it. Indeed cosmological hydrodynamical simulations that model the formation of the MW suggest that it had already accreted most of its dark matter and baryonic mass between $z = 1$ and $z = 2$, i.e. between 8 and 10 Gyr ago (Governato et al. 2007). For simplicity, the potential of the host galaxy is thus assumed to have the present-day properties of the MW. We use a static NFW halo with a virial mass of $M_{\rm vir} = 10^{12}$ $M_\odot$. We also add the potential of a stellar disk with mass $M_{\rm D} = 4 \times 10^{10}$ $M_\odot$.

We choose a typical cosmological orbit with apocentre to pericentre ratio of $r_{\rm a}/r_{\rm p} \approx 5$ (e.g. Ghigna et al. 1998). With a fairly small pericentre of 22 kpc the orbit should be quite typical among those of subhaloes falling into the MW halo quite early, around $z = 2$ (Diemand et al. 2007; Mayer et al. 2007).

The simulation was performed using PKDGRAV, a multi-stepping, parallel, tree N-body code (Stadel 2001). The gravitational softening length was 50 pc for stars and 100 pc for dark matter. We used 200 outputs of the simulation saved at equal snapshots of 0.05 Gyr.

3 GALAXY EVOLUTION

3.1 The orbit

The upper panel of Fig. 1 shows the orbit of the simulated dwarf galaxy during its whole evolution projected on the orbital xy plane, the plane of the stellar disk of the host galaxy. The disk of the dwarf was initially oriented perpendicular to the xy plane.

The simulation started at the right-hand side of the Figure, at the apocentre, 120 kpc away from the host galaxy. Numbers correspond to the evolution time in Gyr since the start of the simulation. The simulation ends after 10 Gyr of evolution at the bottom of the Figure. There are 5 pericentre passages during the evolution. Due to lack of dynamical friction all orbits have very similar parameters, except for the in-plane precession which amounts to about 90 degrees per orbit. Small changes are due to the fact that as the dwarf is stripped the matter around it induces small fluctuations on its orbital dynamics. The pericentre distance $r_{\rm p}$ varies from 21.7 kpc to 23.7 kpc, while the apocentre $r_{\rm a}$ from 110.9 kpc to 113.6 kpc. The ratio remains $r_{\rm a}/r_{\rm p} \approx 5$ as for typical cos-

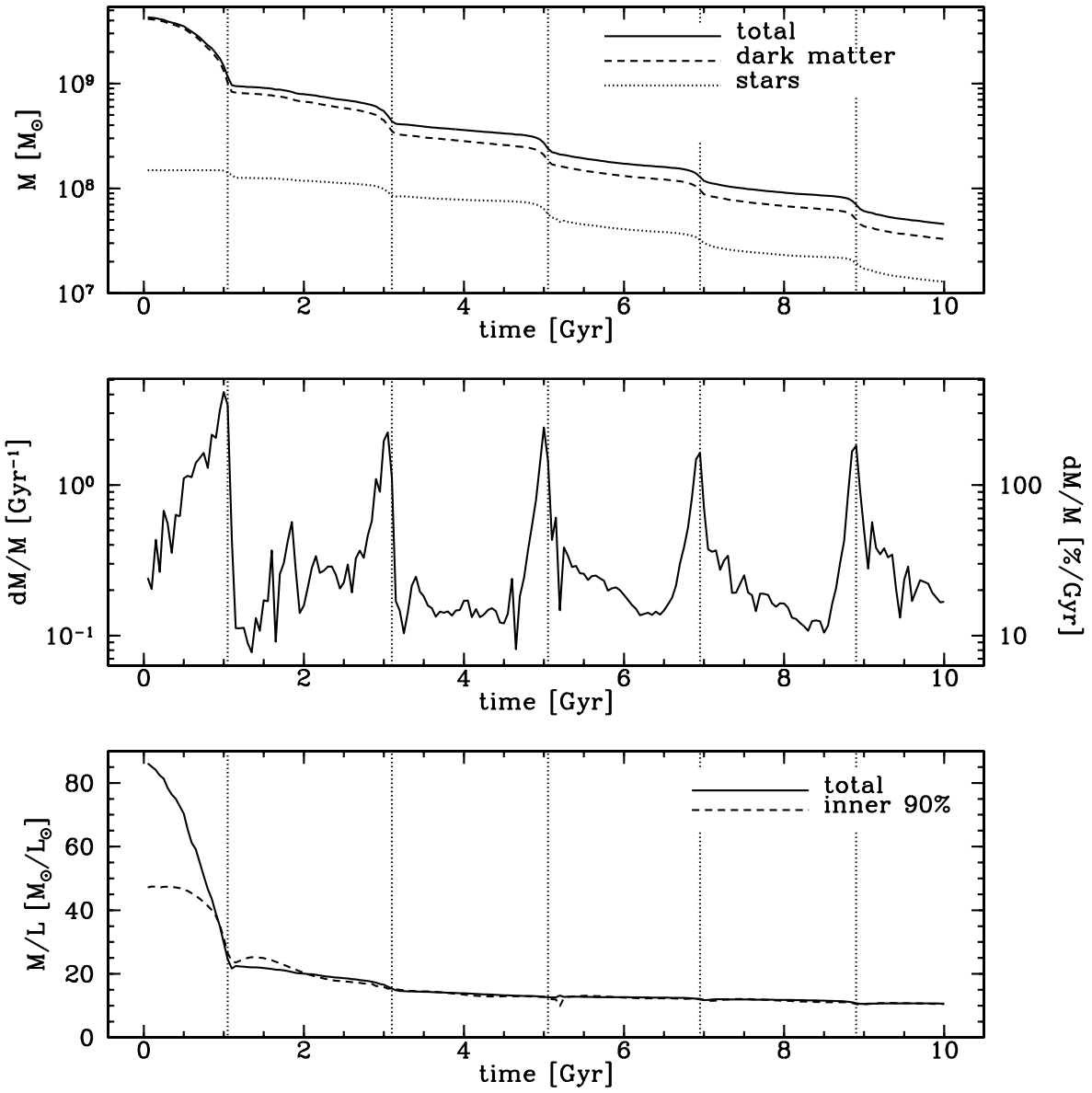

Figure 3. The evolution of the mass and mass-to-light ratio of the dwarf galaxy in time. In the upper panel we plot the mass of all bound particles (solid line), dark matter (dashed line) and stars (dotted line). The middle panel shows the relative mass loss. The lower panel plots the mass-to-light ratio assuming the stellar mass-to-light ratio of 3 solar units. The solid line presents the results for all bound particles, the dashed line plots the same quantity measured inside a sphere containing 90 percent of bound stars. In all panels vertical dotted lines indicate pericentre passages.

mological haloes (e.g. Ghigna et al. 1998). Figure 2 shows the total velocity of the galaxy and its acceleration. All orbit passages are very similar in terms of these parameters, as expected based on the absence of dynamical friction.

3.2 Mass loss

In order to transform a stellar disk into a spheroidal component the galaxy needs to be strongly affected by tides, and several pericentre passages are required in order for that to happen (Mayer et al. 2001, 2007). Prolonged mass loss is unavoidable since each subsequent tidal shock weakens the potential well of the dwarf. The amount of matter lost depends strongly on the orbital parameters and the structural properties of the dwarf galaxy (e.g. Hayashi et al. 2003; Kazantzidis et al. 2004a,b; Peñarrubia, McConnachie & Navarro 2007). As consecutive orbits in the simulation are very similar, the dwarf is affected by a similar tidal field in each orbit. Thus, we can study different stages of the evolution of the dwarf galaxy without the complication of an orbit decaying because of dynamical friction.

In order to calculate the bound mass we need to define the bound particle. For simplicity we decided to treat the dwarf galaxy as an isolated object and define unbound particles as the ones with velocity greater than the escape velocity from the gravitational potential of the dwarf galaxy.

In order to speed up the calculations we used the treecode to estimate gravitational potentials for all particles in all snapshots.

The upper panel of Fig. 3 shows the mass of the galaxy as a function of time, while the middle panel of this Figure shows the relative change of the total mass. Mass loss increases dramatically at the pericentres due to tidal shocking. For example, during the second pericentre passage in a very short time three times more matter is lost than during the rest of the whole second orbit. The first pericentre passage is even more devastating, stripping more than two-thirds of initial galaxy mass. Eventually, after 10 Gyr of evolution 99 percent of the initial mass is lost from the dwarf. This is consistent with analytical models of the initial tidal truncation and subsequent tidal shocks (Taylor & Babul 2001; Taffoni et al. 2003).

The lower panel of Fig. 3 plots the mass-to-light ratio calculated assuming the stellar mass-to-light of 3 $M_\odot/L_\odot$. This should be true for the present time, but not necessarily for the whole evolution since the dwarf might undergo periodic bursts of star formation (Mayer et al. 2001). However, for dwarfs falling in early, 10 Gyr ago as assumed here, most of the gas will be quickly stripped by ram pressure aided by the cosmic ionizing background radiation (Mayer et al. 2007), so that star formation will cease soon after the dwarf approaches the MW. We present the values obtained by dividing the total bound mass by the total light as well as the values measured inside the radius containing 90 percent of the bound stars. We can see that in both cases the ratio decreases rapidly in the early stages, as the extended dark matter halo is disrupted easily while not many stars are lost. Note however that during the subsequent evolution the stellar mass loss traces the mass loss of dark matter. Starting from the second pericentre passage the mass-to-light ratio decreases slowly and relaxes at the value of about 10, remaining constant till the end of the simulation.

3.3 The circular velocity

Although the bound mass is a real physical parameter it is more convenient to express the mass in terms of the maximum circular velocity of the galaxy $V_{\rm max}$, which, as we show below, is also closely related to the stellar velocity dispersion. This is the standard method used in cosmological simulations (e.g. Moore et al. 1999; Kravtsov et al. 2004a; Diemand et al. 2007). It is based on the assumption that $V_{\rm max}$ changes less than other subhalo parameters during its evolution, making it a good choice for tracking subhaloes themselves. Figure 4 shows the profiles of the circular velocity $V_{\rm c} = [GM(r)/r]^{1/2}$ of the dwarf at the six apocentres with dots marking the maximum values $V_{\rm max}$. The upper panel of Fig. 5 shows the evolution of $V_{\rm max}$ in time and the radius $r_{\rm max}$ at which this velocity occurs.

It is interesting to note the main difference between $V_{\rm max}$ and the total bound mass. While the bound mass decreases during the whole evolution, $V_{\rm max}$ remains rather constant between the pericentre passages, decreasing only shortly after the passage, at the time when the tidal tails are formed. This suggests that $V_{\rm max}$ may be a better measure of the mass as it is not affected by the formation of tidal tails farther out. On the other end, $V_{\rm max}$ decreases by almost a factor of 3 during the orbital evolution, similar to the case of the most heavily stripped dark matter subhaloes in Kazantzidis et al. (2004b) and Kravtsov et al. (2004a). This happens despite the presence of the baryons which tend to moderate the effect of tidal shocks by making the potential well deeper, especially once bar formation occurs (see below and Mayer et al. 2007). Hence, for subhaloes that have fallen in early and completed several orbits with fairly small pericentre passages, $V_{\rm max}$ is expected to evolve significantly. This confirms that although haloes of present-day dSphs are consistent with having $V_{\rm max}$ in the range $15 - 30$ km s^{-1} (Kazantzidis et al. 2004b; Strigari et al. 2007) they were much more massive in the past when they entered the MW halo. Such massive dwarfs were likely not affected by reionization, contrary to some suggestions (Grebel, Gallagher & Harbeck 2003).

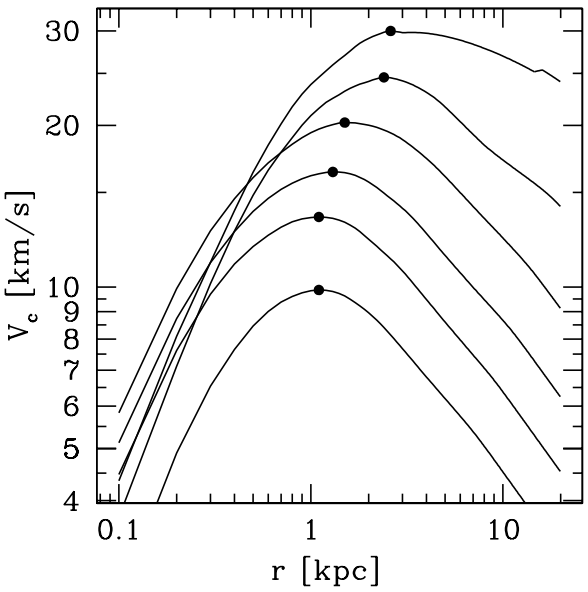

Figure 4. Circular velocity profiles of the dwarf galaxy at apocentres. The highest curve is for the first apocentre (beginning of the simulation), the lowest for the last (end of the simulation). Dots indicate the maximum values $V_{\rm max}$.

The left panel of Fig. 6 shows the relation between $V_{\rm max}$ and the total bound mass $M_{\rm bound}$ during the entire course of dynamical evolution. The solid line presents the whole evolutionary path and the dotted one the relation $M_{\rm bound} \propto V_{\rm max}^{\alpha}$, where $\alpha = 3.5$. Remarkably, although during the 10 Gyr of evolution the dwarf galaxy loses ~ 99 percent of its mass and its $V_{\rm max}$ decreases by a factor of 3, the galaxy moves roughly along the $M_{\rm bound} \propto V_{\rm max}^{3.5}$ line. As expected, the largest (smallest) deviations from this relation occur at orbital pericentres (apocentres). Our findings are in agreement with Hayashi et al. (2003) who found that $M_{\rm bound} \propto V_{\rm max}^{3}$ in numerical simulations of tidal stripping of *pure* NFW subhaloes and Kravtsov et al. (2004a) who reported a value of $\alpha = 3.3$ for stripped dark matter subhaloes in cosmological N-body simulations.

A similar comparison can be made in terms of the stellar mass instead of the total bound mass. The right panel of Fig. 6 shows the relation between the total luminosity of the stars and $V_{\rm max}$, $L \propto V_{\rm max}^{\alpha}$. The luminosity was calculated using the bound stellar mass and assuming a mass-to-light ratio of the stellar component of 3 $M_\odot/L_\odot$ as before. This

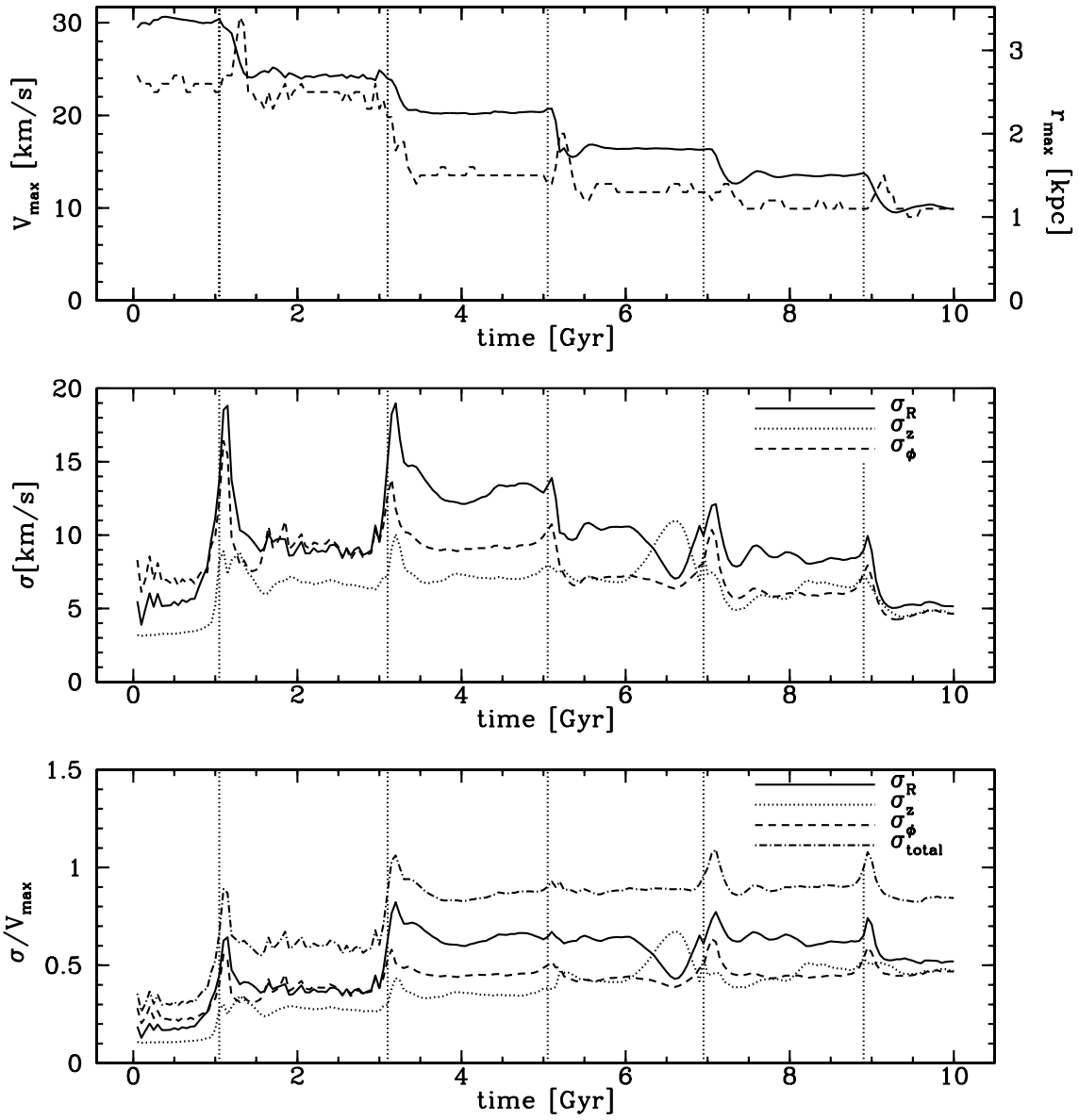

Figure 5. Upper panel: the maximum circular velocity (solid line, left axis) and the radius at which the maximum circular velocity occurs (dashed line, right axis). Middle panel: velocity dispersions of the bound stellar particles of the dwarf galaxy measured in cylindrical coordinates. Lower panel: the same velocity dispersions expressed in units of the maximum circular velocity. Also the total velocity dispersion is shown in this case. In all panels vertical dotted lines indicate pericentre passages.

time the power-law relation is followed only in the intermediate stages with $\alpha = 3$, while it flattens in the beginning and at the end of the simulation. A similar comparison was done by Kravtsov et al. (2004b) for dark matter haloes in their N-body simulations. They used SDSS luminosity function to predict stellar luminosities in the R band for their haloes. In the range 100 km s^{-1} $< V_{\rm max} <$ 200 km s^{-1} their relation also follows a power-law with $\alpha = 3$. It would be difficult to compare exact fits of the relation as one would need to apply proper bolometric corrections, which differ for different types of stars.

3.4 Internal kinematics

The middle panel of Fig. 5 shows the evolution of the velocity dispersions of the bound stellar particles measured in cylindrical coordinates R, z and ϕ. The z axis is always along the total angular momentum vector of the stars thus the R-ϕ is the rotation plane. All velocities were projected on a given axis and their mean values were computed (so for example for the ϕ direction the mean is the average rotation velocity V_ϕ). Then the dispersions were calculated for all bound stellar particles with respect to the corresponding mean values. It is interesting to note that all three velocity dispersions relax very quickly after the pericentre and remain roughly constant for the rest of the orbit. This suggests that the

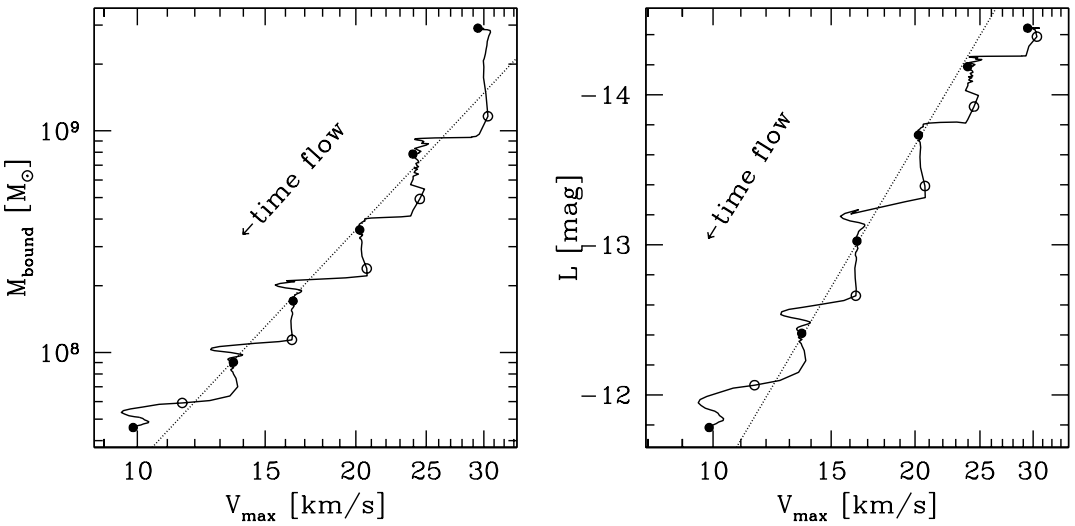

Figure 6. Mass-maximum circular velocity relations. The left panel shows the total bound mass versus the maximum circular velocity for the whole evolutionary path of the dwarf galaxy (solid line). The dotted line corresponds to the relation $M_{\rm bound} \propto V_{\rm max}^{3.5}$. The right panel shows the mass of the stellar component expressed in terms of the bolometric magnitude (assuming the stellar mass-to-light ratio of 3 solar units) as a function of the maximum circular velocity, with dotted line corresponding to the relation $L \propto V_{\rm max}^{3}$. In both panels apocentres are marked as filled circles and pericentres as open circles.

galaxy relaxes very quickly to a new equilibrium configuration and can thus be successfully modelled using the virial theorem or the Jeans equations for most of the time (Klimentowski et al. 2007).

Combining the results shown in the two upper panels of Fig. 5 we can study the relation between the stellar velocity dispersion and the maximum circular velocity $V_{\rm max}$ of the simulated dwarf. This relation is used to construct cumulative velocity functions of dwarf galaxies in the Local Group. Comparisons with the corresponding functions of dark matter satellites in galaxy-sized dark matter haloes gave rise to the missing satellites problem. However, the velocity functions of satellites depend sensitively on the particular assumptions made to infer $V_{\rm max}$ from observations. For example, Moore et al. (1999) adopted an isothermal halo model with a flat circular velocity profile, while Kravtsov et al. (2004a) used circular velocities measured either from the rotation curve or from the line-of-sight velocity dispersion, assuming isotropic velocities. All these simulations lacked the baryonic component, while here we can assess directly the relation between $V_{\rm max}$ and the stellar velocity dispersion. The ratio of the two quantities is plotted in the lower panel of Fig. 5. It turns out that $V_{\rm max}$ traces very well each of the measured velocity dispersions as well as the total velocity dispersion $\sigma_{\rm total} = (\sigma_R^2 + \sigma_z^2 + \sigma_\phi^2)^{1/2}$ for most of the time except just after the pericentres.

Dwarf spheroidals are low-angular momentum systems, as highlighted by their low ratio of the rotation velocity to the velocity dispersion, V_ϕ/σ (Mateo 1998). It is thus important to study the angular momentum evolution of a tidally stirred disky dwarf. The solid and dashed line in the upper panel of Fig. 7 show the mean angular momentum of the stellar and dark matter particles, respectively. In the lower panel of the Figure the dashed line shows the angle γ between the total stellar angular momentum vector and the orbital plane (right axis). The angular momenta were calculated for the inner core (bound particles within $r < 1.5$ kpc from the centre) and were expressed in units of the initial values. The initial angular momentum for stars is 2925 $M_\odot$ kpc km s^{-1} per particle, for particle mass of $M_{\rm star} = 150$ $M_\odot$. The initial angular momentum of dark matter particles equals 82800 $M_\odot$ kpc km s^{-1} per particle, for particle mass of $M_{\rm DM} = 1035$ $M_\odot$. The solid line in the lower panel of Fig. 7 presents the ratio of the mean rotation velocity of bound stars to the total stellar velocity dispersion. We see that the ratio decreases systematically, except for a slight increase after the last pericentre.

Let us look closer at the evolution of the kinematics. After the first pericentre passage only very little angular momentum is lost. The radial velocity dispersion σ_R rises slightly, but this is not enough to transform the disk. An elongated disk is created with higher radial dispersion. This object is not very stable and after the second pericentre passage it is transformed into a bar. More than half of the angular momentum is lost and the radial velocity dispersion rises dramatically. At this stage radial orbits dominate the elongated bar, but still circular orbits are present. During the following pericentre passages the angular momentum is transferred outside the galaxy, slowing down the rotation.

After the fourth pericentre passage almost all angular momentum is lost. At this stage radial orbits dominate and there is almost no rotation. Interestingly, the fifth pericentre passage differs from the earlier ones. This time some angular momentum is added into the galaxy while the radial velocity dispersion is strongly reduced (note that the upper panel of Fig. 7 shows only the mean angular momentum, thus increase of angular momentum could actually mean the removal of particles with no angular momentum). In the end, a spheroidal galaxy forms with velocity dispersions equal in all directions and some internal rotation. During the evolution not only the amount of angular momentum was changed. The angle between the angular momentum vector and the

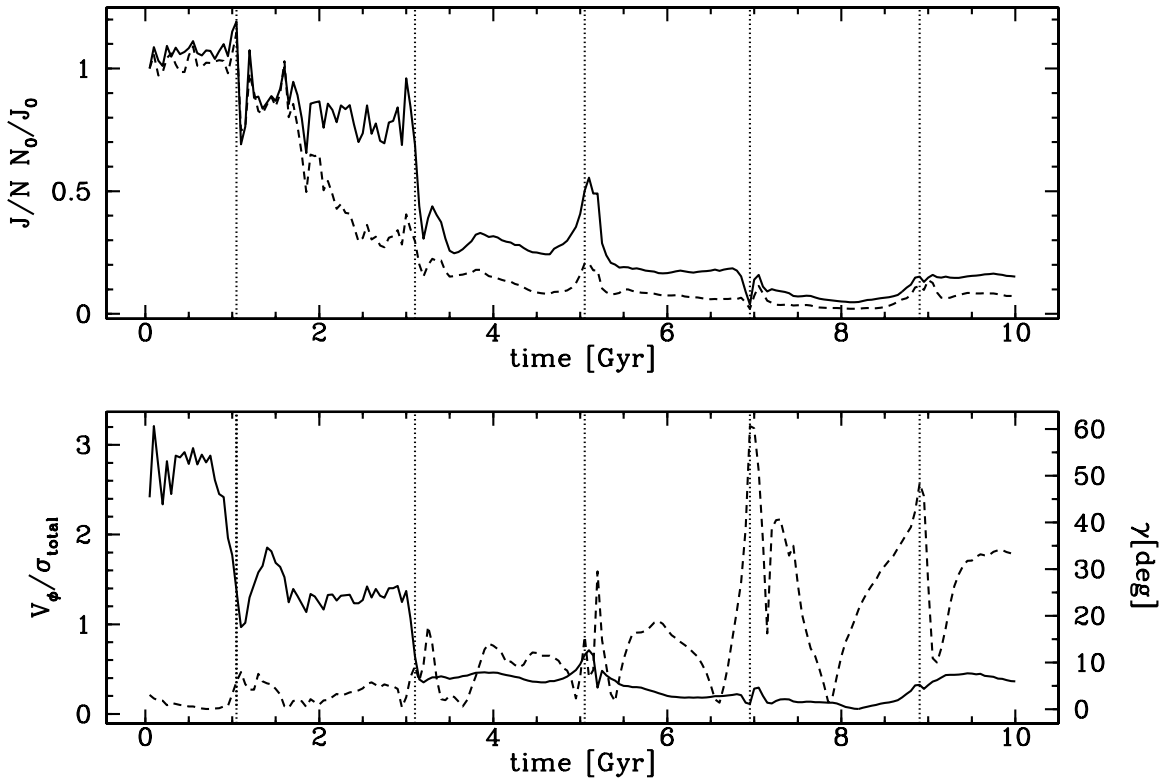

Figure 7. The upper panel shows the scaled mean angular momentum of the stellar particles (solid line) and dark matter particles (dashed line). The lower panel plots the ratio of the rotation velocity of the stellar particles to their total velocity dispersion (solid line, left axis) and the angle γ between the total angular momentum vector of the stars and the orbital plane (dashed line, right axis). In both panels vertical dotted lines indicate pericentre passages.

orbital plane plotted in the lower panel of Fig. 7 (dashed line) shows that the rotation plane, which was initially perpendicular to the orbital plane (angular momentum vector parallel to the plane), deviates by around 30 degrees by the end of the evolution.

According to the picture presented here, the rotating bar seems to be stable as long as angular momentum is transferred outside. After almost all angular momentum is removed, a spheroidal galaxy is created. Depending on the efficiency of this process, a spheroidal galaxy may require more or less time to form or smaller/larger number of pericentres. It also suggests that newly created spheroidal galaxies could possess some rotation which they had gained in previous pericentre passages. It is not clear whether this rotation would be suppressed during further evolution. We refrain from considering this a general result as it is based on only one simulation. Indeed, Mayer et al. (2001) showed that a range of final V_ϕ/σ and structural properties can be obtained by varying the initial dwarf model and the orbit.

We also note that no bar buckling occurs in this simulation. Bar buckling which isotropizes the velocity ellipsoid and puffs up the stellar bar was identified as the main mechanism responsible for the formation of a dSph in the case of high surface brightness dwarfs (Mayer et al. 2001). A similar result was found for the transformation of relatively massive and bright dwarfs in galaxy clusters (Mastropietro et al. 2005). Therefore, it would seem that there are at least two channels of dSph formation, tidal heating and shocking of the bar and bar buckling. The first scenario applies to low surface brightness dwarfs as the one studied in this work. This mechanism likely is the dominant one for producing faint dSphs such as those of the Local Group (see also Mayer et al. 2007). On the other hand, buckling requires a strong bar and thus a fairly high surface brightness system.

There is no angular momentum transfer in the inner parts of the dwarf between the stellar component and the dark matter halo. Both quantities in the upper panel of Fig. 7 display similar behaviour (except for the time between 2 and 3 Gyr). During the first two pericentre passages, the outer parts of the bound dark matter halo gain angular momentum from the stellar particles, but it is quickly transferred outside and then lost as the outer halo gets stripped. Therefore bound dark matter particles do not accumulate angular momentum like haloes in barred spiral galaxies (Athanassoula 2002). Angular momentum is instead transferred directly outside to the tidal streams.

3.5 The shape of the dwarf

Fig. 8 shows the evolution of the shape of the stellar component of the dwarf as a function of time. In the upper panel we show the ratios of the principal axes lengths computed from the eigenvalues of the moment of the inertia tensor using the method described by Kazantzidis et al. (2004c) at the radius of the maximum circular velocity (see Fig. 5). The choice of this radius is justified as it is large enough to trace the shape

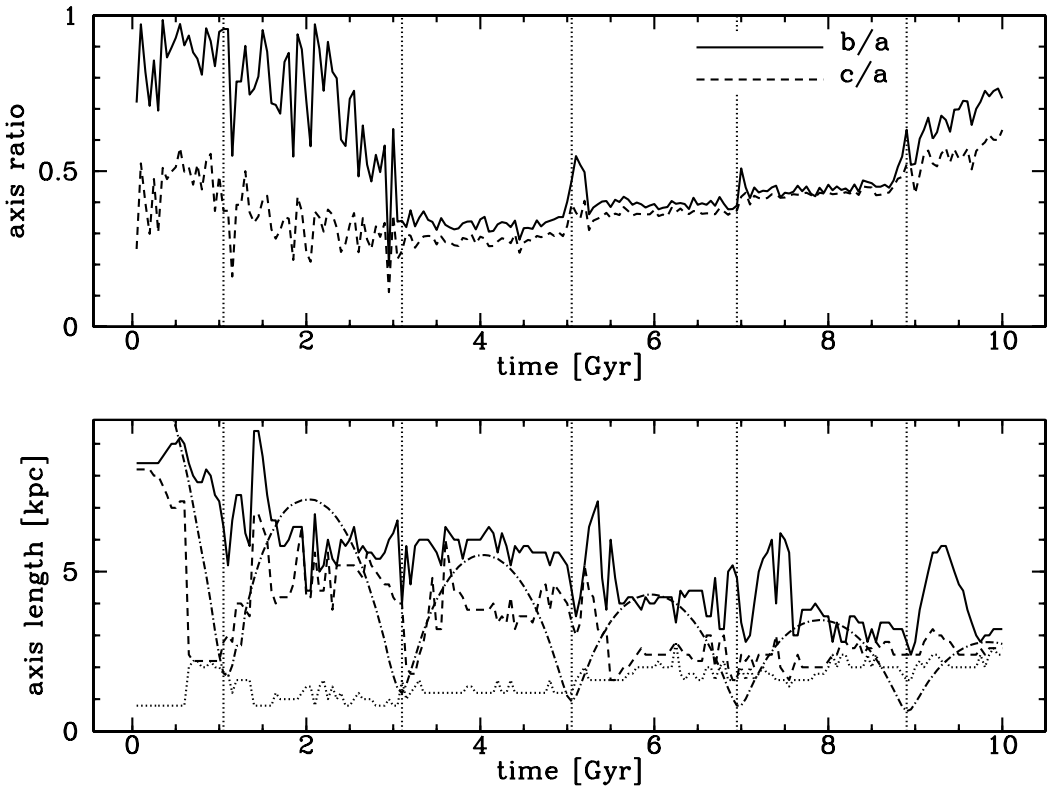

Figure 8. The evolution of the shape of the stellar component of the dwarf in time. In the upper panel the shape is described by the ratios of the lengths of principal axes measured at the radius of maximum circular velocity (with a, b, c being the longest, middle and shortest axis respectively). In the lower panel we plot the axes lengths estimated by enclosing 95 percent of the total bound mass. The dotted line corresponds to the shortest axis, the dashed and solid lines are for the middle and longest axis. The dotted-dashed line shows the approximate tidal radius of the system estimated from equation (1). In both panels vertical dotted lines indicate pericentre passages.

of the bound component of the galaxy, while small enough to avoid contamination from the tidal tails. In the lower panel, we present the lengths of the axes estimated by considering a cuboid with a cross-section of 0.2×0.2 kpc and increasing its length which follows the principal axis vector. By increasing its size we enclose a progressively larger fraction of the bound mass of the galaxy. We stop the procedure when 95 percent of the total (bound) mass which can be enclosed is inside. The length of the axis is equal to the length of the cuboid. The dotted-dashed line shows the Jacobi limit of the dwarf galaxy which approximates its tidal radius (Binney & Tremaine 1987):

$$r_t = D \left[\frac{m}{M(3 + m/M)} \right]^{1/3} \quad (1)$$

where m is the mass of the dwarf, M is the mass of the host galaxy and D is the distance between the dwarf and the host.

The formation of a dSph galaxy out of a disk-like system appears to be a long and complicated process. Fig. 8 shows that at the beginning the stellar component is a highly flattened disk (with two equal long axes and a short one). After the first pericentre passage matter is not removed isotropically from the disk. Clearly, the length of only one axis is reduced. The disk becomes thicker and triaxial. During the second pericentre passage the disk is turned into a bar with only one long axis. Afterwards the bar is rather stable and little affected by the next pericentre passages. Matter is mostly removed from the outer ends of the bar, thus the longest axis shortens in time (the axis ratio increases slightly) and the bar becomes thicker. Eventually, after the fifth pericentre passage the morphology of the dwarf changes dramatically: the bar dissolves and the stars form a triaxial shape with axes of comparable size.

At the end of the simulation, the newly formed dSph galaxy is characterized by the following properties of the stellar component:

(i) low ratio of the rotation velocity to the total velocity dispersion, $V_\phi/\sigma_{\rm total} \leq 0.5$,
(ii) a spheroidal shape with axis ratios $b/a = 0.75$ and $c/a = 0.6$,
(iii) isotropic velocity distribution, $\sigma_R \approx \sigma_z \approx \sigma_\phi$.

3.6 The last pericentre passages

According to the analysis of the previous subsections, the pericentre passages are the most eventful parts during the orbital evolution of the dwarf galaxy. As already mentioned, the strength of the tidal forces acting on the dwarf is essentially the same at each pericentre passage in our simulation since there is no orbital decay due to dynamical friction. A question thus arises: why does the bar survive the third and

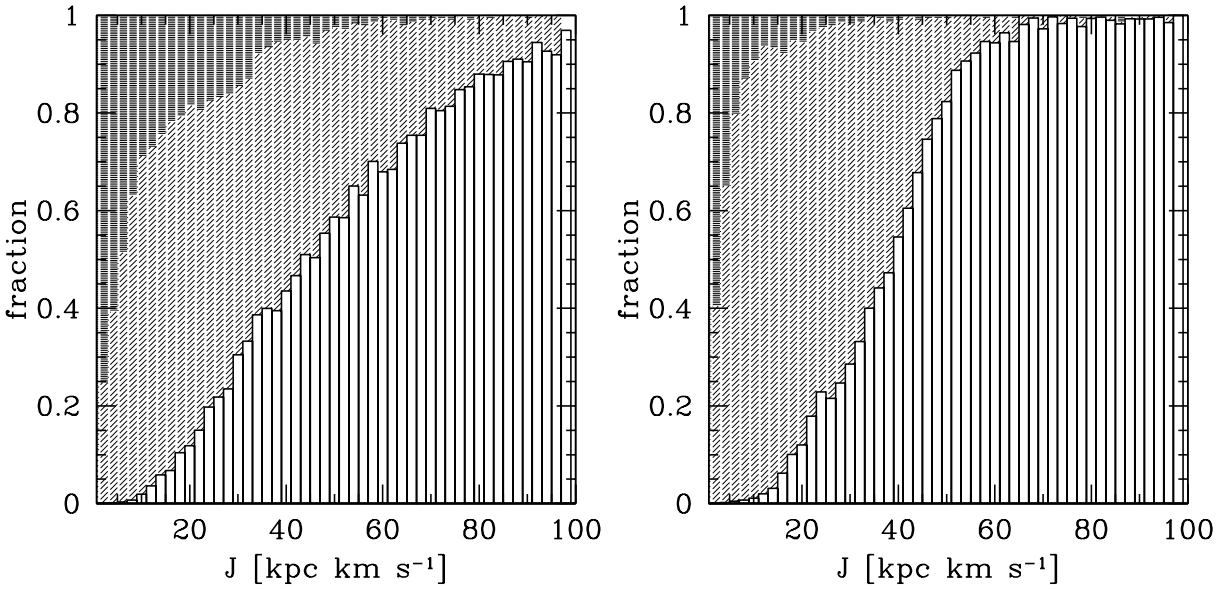

Figure 9. Comparison between the fourth and the fifth pericentre passage. The left diagram corresponds to the fourth pericentre passage, the right one to the fifth. They show probabilities that a bound stellar particle with a given angular momentum before the pericentre passage escapes from the dwarf (lower open region), gains angular momentum but remains bound (middle lightly shaded region) and loses angular momentum (upper strongly shaded region).

fourth pericentre passages while it is suddenly turned into a stellar spheroid at the fifth pericentre passage?

The evolution of the angular momentum shown in the upper panel of Fig. 7 addresses this question at least partially. In order to preserve a bar one has to transfer angular momentum outside. Lowering angular momentum makes the orbits more radial, thus the bar gets stronger (Athanassoula 2002). During the fifth passage some angular momentum is added into the dwarf destroying the bar. Stellar orbits typically become more circular and the galaxy more spherical.

In order to study the mechanism of this transformation we marked a representative group of particles and followed their orbits during the evolution measuring their properties. Figures 9 and 10 show the results of this study. The left diagram in Fig. 9 corresponds to the fourth pericentre passage while the right one to the fifth. They illustrate the probabilities that a bound particle with a given angular momentum before the pericentre passage escapes from the dwarf (lower open region), gains angular momentum but remains bound (middle lightly shaded region) and loses angular momentum (upper strongly shaded region). The three left panels of Fig. 10 show the number of bound stellar particles with a given angular momentum and energy in the apocentres before the fourth (upper), before the fifth (middle), and after the fifth pericentre passage (lower). The two diagrams in the right column show the corresponding values for the stars in the bar. This Figure answers the question why the mean angular momentum changes while Fig. 9 shows how exactly this change occurs.

According to the upper panel of Fig. 7 during the fourth pericentre passage stellar particles lose angular momentum on average. Comparison between the upper left and the middle left panel of Fig. 10 confirms this picture. Most particles fill the low angular momentum regions of the $J-E$ plane in both panels ($J < 6$ kpc km s^{-1}). These regions correspond to the bar as verified by the two diagrams in the right column which show explicitly the results for stars in the bar. The main difference is due to the high angular momentum particles (top-right part of the diagrams), which escape from the dwarf easily during the fourth pericentre passage. This on average lowers the mean angular momentum of particles significantly.

The fifth pericentre passage is very different from the fourth. According to the lower left panel of Fig. 10 after the fifth pericentre passage the majority of particles occupies the region of higher angular momentum ($J \approx 10$ kpc km s^{-1}) and higher energies, while the region with low-E and low-J particles that formed the backbone of the bar has vanished. By inspection of the right diagram of Fig. 9 we find that indeed some of the low-J particles escape from the dwarf but most of them only gain angular momentum while remaining bound. There are much fewer particles that lose angular momentum. In general particles from lower-J orbits take place of the higher-J particles which escaped. This way the number of low angular momenta particles lowers, while the number of particles with momenta higher than 5 kpc km s^{-1} remains roughly the same. The end result is that the average angular momentum per particle rises.

It seems that in order to create a spheroidal galaxy an increase of the angular momentum of particles beyond some critical value must occur. Such increase of angular momentum somehow replaces the orbit families needed to support a bar with different, more circular orbits. While in the bar stage the majority of particles have very low angular momenta, in the spheroidal stage the majority of the particles have angular momenta close to the maximum possible for a bound orbit (top of the distribution). It is not clear why such an inversion occurs during the fifth pericentre passage. Note that, despite the increase of angular momentum in this last phase, the final angular momentum of the galaxy is about

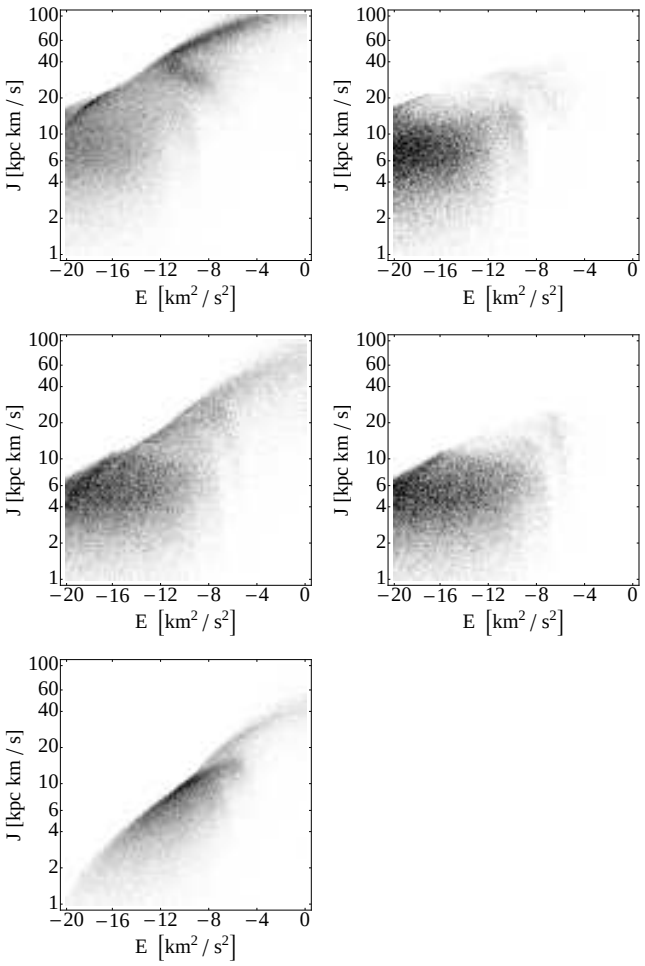

Figure 10. The distribution of bound stellar particles in the energy-angular momentum plane (darker shading corresponds to the higher density of particles) for the apocentre preceding the fourth (upper panels), preceding the fifth (middle panels) and following the fifth pericentre passage (lower panel). The left-column diagrams show the results for all bound stellar particles, the right ones only for the stars in the bar. No diagram is plotted in the lower right corner because the bar is destroyed by this stage.

one order of magnitude lower than it was at the beginning of the evolution (see Fig. 7). As a result, $V_\phi/\sigma_{\rm total} \leq 0.5$ even at the end, as expected for a true dSph galaxy. The evolution of the angular momentum in the upper panel of Fig. 7 suggests that almost all angular momentum must be removed before the transformation occurs, but it is not clear whether that is a sufficient condition. The alignment of the total angular momentum vector with respect to the orbital velocity of the dwarf could be another factor.

We repeated the same analysis but distinguishing the particles with prograde and retrograde orbits inside the dwarf with respect to the orbit of the galaxy around the MW. Prograde orbits were defined for positive values of the scalar product of the angular momentum of the particle (calculated with respect to the centre of the dwarf galaxy) and the whole galaxy (calculated with respect to the centre of the host galaxy). There was no significant difference between these two cases which suggests that the direction of motion of a given particle does not influence its future evolution. This means that it is not the orbit alignment (for example with respect to the angular momentum vector) which causes the bar to transform into the spheroidal.

4 TIDAL TAILS

Matter stripped from the dwarf galaxy will form tidal tails which will eventually become completely unbound and form tidal streams tracing the original orbit of the dwarf in the MW halo. The presence of tidal tails around observed dSph galaxies is very probable. Martínez-Delgado et al. (2001) found tidal extensions in Ursa Minor and Coleman et al. (2005) showed differences in surface brightness around Fornax depending on the line of sight. Tidally induced overdensities in the distribution of stars were also detected around Carina (Muñoz et al. 2006) and Leo I (Sohn et al. 2007). Klimentowski et al. (2007) showed that stars originating from tidal tails can contaminate kinematic samples of dSph galaxies leading to significantly overestimating their velocity dispersions. Overall, owing to their low surface brightness, tidal tails are still very difficult to detect by photometric techniques. In what follows, we only investigate the properties and dynamics of the stellar tidal tails in the N-body simulation.

4.1 The orientation of tidal tails

The first interesting question about tidal tails is whether there is a correlation between their orientation and the orbit of the dwarf galaxy. If such correlation exists it would help to study dSph orbits and serve as a complement to proper motions measurements which still have rather large errors (e.g. Piatek et al. 2007).

The alignment of the tidal tails in the simulation was calculated for all stellar particles, starting from the beginning of the tail near the dwarf up to 10 kpc from the galaxy by fitting a straight line to the direction where the density along the tails reaches a maximum. The lower panel of Fig. 1 plots the orbit of the simulated dwarf galaxy during its whole evolution (solid line) with dotted lines showing the direction of the tidal tails at a given position on the orbit. There are always two tidal tails emanating from the two opposite sides of the galaxy. While the two tails are not always equilinear (they rarely intersect the centre of the galaxy), they are always parallel to each other. That is why the direction of both tails can be represented by a single straight line. At some specific locations of the orbit there were no clear tidal tails visible (as indicated by the lack of dotted lines). Such behaviour occurred around 4 Gyr after the beginning of the simulation (left part of Fig. 1), when matter was rather uniformly distributed around the dwarf.

According to Fig. 1 tidal tails are parallel to the orbit only in very short periods of time preceding the pericentres. In the outer parts of the orbit, near apocentre (where the dwarf galaxy spends most of its time) tidal tails always point almost radially towards the host galaxy. This behaviour is in agreement with Montuori et al. (2007) who found the same effect in their N-body simulations of globular clusters. Therefore tidal tails in the immediate vicinity of the galaxy cannot be used to directly determine the orbit. Only completely unbound stars, forming tidal streams further out

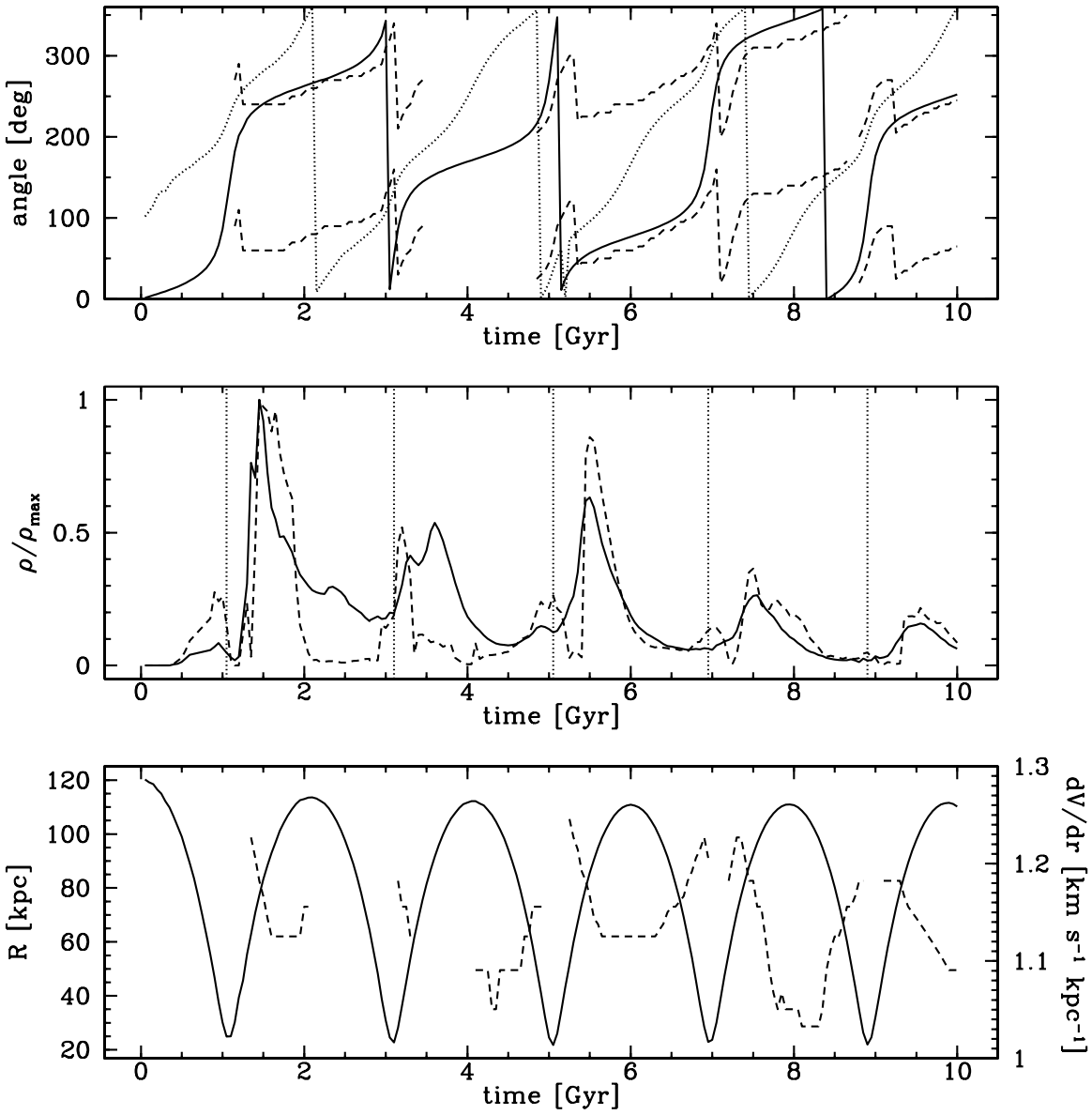

Figure 11. Properties of the tidal tails. The upper panel describes the direction of the tails. The solid line corresponds to the angle between the position vector of the dwarf galaxy and a fixed x axis. The dotted line shows the angle between the velocity vector of the dwarf and the same axis. Dashed lines correspond to the angle between both tidal tails and the fixed axis. The middle panel shows the density of the tidal tails. The solid line corresponds to the mean density of all matter at the distance of 10 kpc from the dwarf (calculated in a ring of 1 kpc in size), while the dashed line shows the same density but measured on the axis of the tails (calculated in two boxes with 1 kpc on a side placed at 10 kpc from the centre of the dwarf in opposite directions). Densities are plotted relative to their respective maximum values. Vertical dotted lines indicate pericentre passages. The lower panel shows the values of $\mathrm{d}V/\mathrm{d}r$, the slope of the relation between the velocity of particles in the tidal tails and their distance from the dwarf (dashed line) fitted to velocity diagrams similar to Fig. 15 along with the distance of the dwarf from the host galaxy (solid line) as a function of time.

from the bound component of the dwarf, tend to follow the orbit.

The upper panel of Fig. 11 presents the same results in a more quantitative way by comparing the angle between the tidal tails and a fixed axis to the angle between the direction to the host galaxy and the velocity vector and the same axis. Tidal tails tend to be oriented radially: their direction is similar to the direction of the dwarf's position vector for most of the time. Only for a short time around the pericentre they are roughly parallel to the velocity vector. This result is illustrated further in Fig. 12 where we plot in the upper panel the angle between the direction towards the centre of the MW and the nearest tidal tail during the last 4 Gyr of evolution (the last two orbits, 80 simulation outputs) where the tails are easily identifiable. The lower panel of this Figure presents the distribution of the angle which shows a strong peak for low angles of $0^\circ - 30^\circ$.

The radial alignment of tidal tails may at least partially

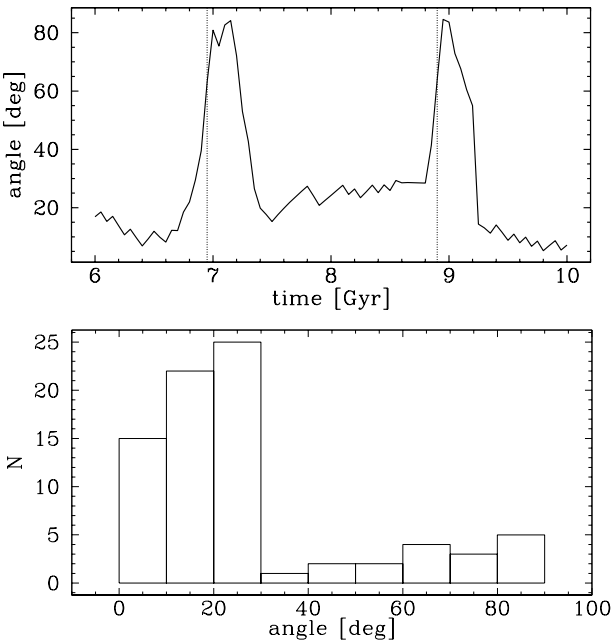

Figure 12. The angle between the direction to the MW centre and the nearest tidal tail of the dwarf galaxy as a function of time (upper panel) and its distribution (lower panel). The results come from 80 simulation outputs corresponding to the last two orbits or the last 4 Gyr of evolution.

explain the difficulty of detecting them by photometric observations. Since we are looking at the dwarfs from the inside of the MW their tidal tails are most probably oriented along the line of sight and they would be usually confused with a much brighter dwarf galaxy itself. The kinematic samples of stars in most dSph galaxies might thus be contaminated by unbound stars from the tails. It is therefore essential to remove these unbound stars in order to get reliable mass estimates for dwarf galaxies (Klimentowski et al. 2007). On the other hand, when the line of sight is perpendicular to the tidal tails the tails will generate an excess of star counts at a few core radii from the centre, which will show up as a flattening of the outer part of the star counts profile (Klimentowski et al. 2007). Such flattening might have been observed in some dSphs but not in all of them (Muñoz et al. 2006; Muñoz, Majewski & Johnston 2008).

The lower panel of Fig. 1 and the upper one of Fig. 11 show that while the transition from the radial to the orbital (i.e. parallel to the orbit) orientation of the tidal tails happens rather smoothly when the dwarf approaches pericentre, the transition from the orbital to the radial orientation after a pericentre passage is rather abrupt. This is best visible after the third and the fifth pericentre passage and happens roughly halfway between the pericentre and the apocentre over a very short timescale. Figures 13 and 14 present three snapshots from the simulation showing this remarkable transition starting at 5.15 Gyr after the beginning of the simulation. Previously formed tidal tails, perpendicular to the radial direction (towards the host galaxy) are destroyed shortly after the pericentre passage by tidal forces, and then new, radially aligned tidal tails are produced very quickly. We refer to this phenomenon as the 'tidal tail flipping'.

4.2 The dynamics of tidal tails

The middle panel of Fig. 11 shows the relative density of stars in the tidal tails at the distance of 10 kpc from the dwarf galaxy (dashed line) compared to the density everywhere around the galaxy (measured in a ring, solid line). In addition to the results concerning the mass loss (Fig. 3) these measurements illustrate the mechanism for tail formation. Most matter is stripped during the pericentre passages but tidal tails enhance their density later on the orbit reaching the maximum density typically about 0.5 Gyr after the pericentre. This is because some time is required for stars to travel several kpc away from the galaxy and form the tails. After reaching the maximum, the density drops exponentially until the next pericentre passage, after which the previously formed tails are dissolved and new tails are formed, as described in the last subsection.

This picture suggests that it would be much easier to detect tidal tails for galaxies with positive radial velocities with respect to the host galaxy (i.e. on their way to the apocentre). The parts of the diagram shown in the middle panel of Fig. 11 where the solid line is higher than the dashed indicate that the tidal tails are then highly diffuse. This is especially well visible around 4 Gyr where no clear tails are formed, while there is a significant number of stars distributed uniformly around the galaxy. This fact suggests that prominent tidal tails are not always present as a dwarf satellite evolves in the primary's potential.

Figure 15 plots velocities of the stellar particles inside the dwarf galaxy and its tidal tails projected on an axis parallel to the tidal tails as a function of the distance from the centre of the dwarf measured along the same axis. Interestingly, there is a clear linear relation between the particle radial velocity and its distance from the galaxy. It turns out that this relation is valid during most of the time except for the pericentre passages. Only the slope of the $V(r)$ relation varies with time.

The particles enclosed between the vertical solid lines in Fig. 15 nearly all have velocities lower than the escape velocity, thus they are still bound to the galaxy and are expected to fall back, while particles outside will eventually feed the tidal streams. The lower panel of Fig. 11 shows with dashed lines the values of $\mathrm{d}V/\mathrm{d}r$ (the slope of the relation) along with the distance of the dwarf from the host galaxy (solid line) as a function of time. The slope of the relation is anticorrelated with the distance from the host galaxy. After the pericentre passage, when the tails are created, the $V(r)$ relation is steeper and it flattens with time. After the apocentre the relation becomes steeper again, until destruction of the tails. The numerical values plotted in the lower panel of Fig. 11 were obtained by fitting a linear function to the velocity diagrams similar to the one presented in Fig. 15 for every simulation output. The fitting was done for the distance range $5 < |r| < 20$ kpc.

It is important to emphasize that the presence of a star in the tidal tails does not imply that it is unbound to the galaxy. Some of the stars from the tidal tails are actually falling back onto the dwarf. The bound region marked by the vertical solid lines in Fig. 15 varies with time. When the dwarf travels from the pericentre to the apocentre unbound stars leave its vicinity quickly, while the fastest bound stars reach their turnaround points shortly after the apocentre.

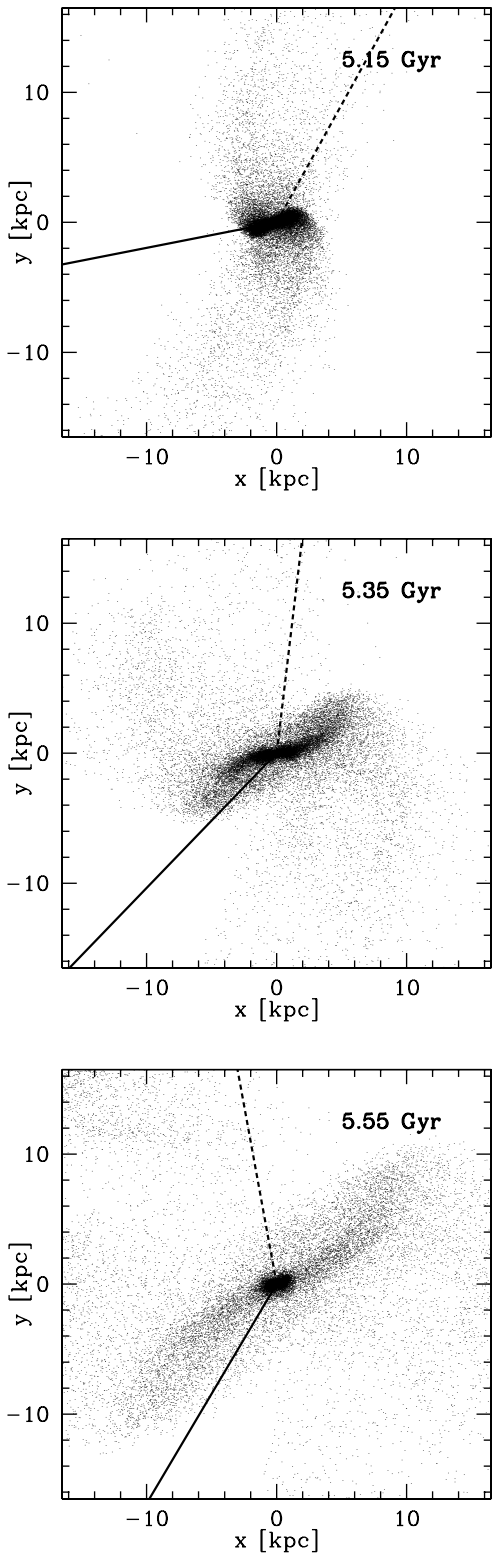

Figure 13. Tidal tail flipping. The three panels show three snapshots from the simulation at 5.15, 5.35 and 5.55 Gyr from the start. Only the positions of stellar particles are shown projected onto the orbital plane. The solid line indicates the direction to the host galaxy while the dashed one is parallel to the velocity vector. Old tidal tails oriented almost along the orbit decay and new ones pointing radially towards the host galaxy are formed.

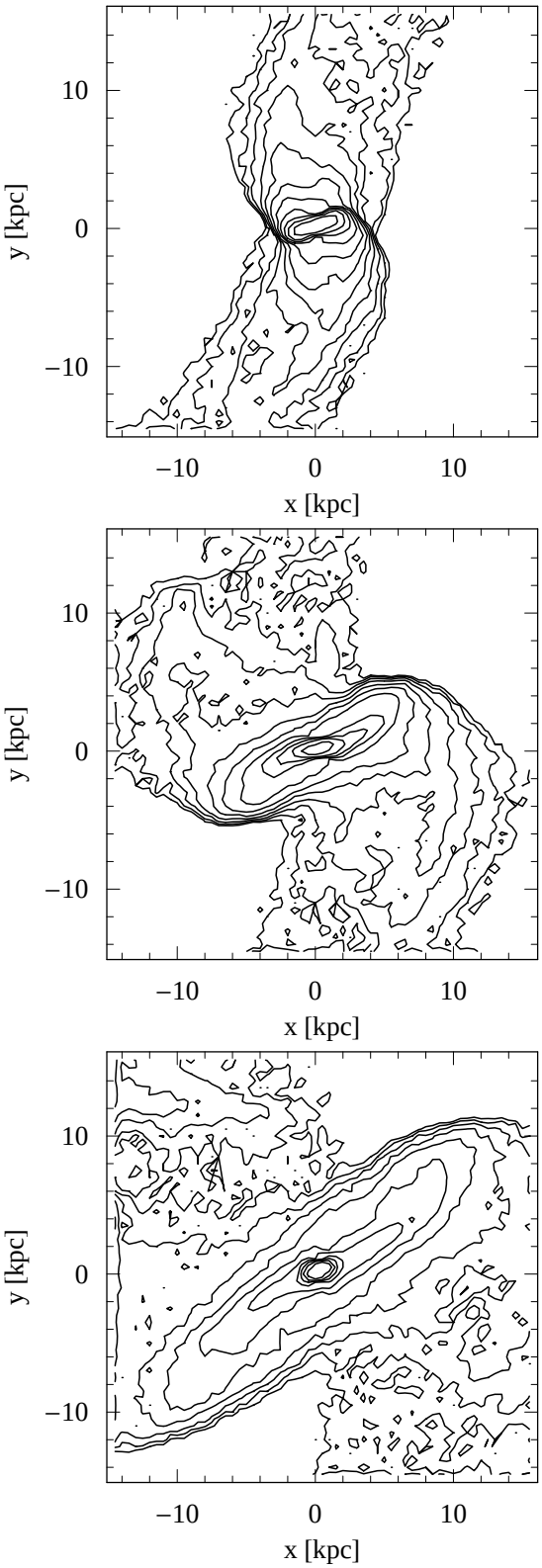

Figure 14. Contour plots of the surface density of stars corresponding to the three stages shown in Fig. 13. Each contour marks the density twice lower than the previous one. Assuming the stellar mass-to-light ratio of 3 solar units, the innermost contour corresponds to 2 $L_\odot$ pc^{-2}, while the outermost to 0.002 $L_\odot$ pc^{-2}.

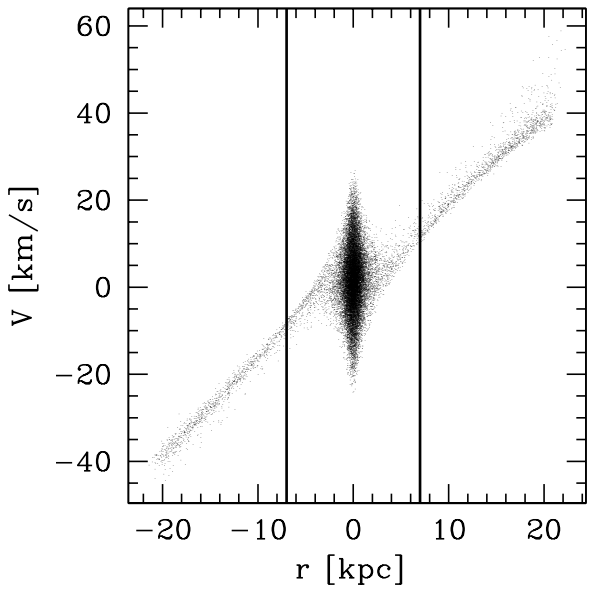

Figure 15. Velocities of stellar particles of the simulated galaxy at $t = 8.5$ Gyr projected onto the axis parallel to the tidal tails (and intersecting the centre of the galaxy). The coordinate r measures the distance from the centre of the dwarf projected onto this axis. Vertical solid lines separate bound stars (between the lines) from the unbound ones (outside).

This extended region, dominated by bound stars, can reach up to 10 kpc from the galaxy.

5 SUMMARY AND DISCUSSION

We have studied the tidal evolution of a two-component dwarf galaxy on an eccentric orbit in the MW potential using a high-resolution N-body simulation. We have conducted a detailed analysis of how a low surface brightness disk-like system similar to present-day dwarf irregulars transforms into a dSph galaxy. The present investigation allows for a quantitative understanding of the transformation which improves considerably on previous work on the subject. Initially, the tidal forces at pericentre trigger bar formation in the disk, which at the same time suffers stripping of its outer region. The rotating bar transfers angular momentum outward. As long as the angular momentum is transferred outside, the bar is preserved. During the fifth pericentre passage, when there is almost no angular momentum left in the bar, the average angular momentum per stellar particle increases slightly and the bar is destroyed. The orbital distribution of the bound stars changes abruptly, nearly radial orbits that constituted the backbone of the bar disappear and are replaced by more circular orbits. A spheroidal galaxy is formed as a result of the bar destruction. This is different from the bar buckling instability identified in Mayer et al. (2001) and Mastropietro et al. (2005) as the mechanism whereby high surface brightness, relatively massive disky dwarfs transform into dSphs.

We find that the stellar disk 1D velocity dispersions trace well the maximum circular velocity $V_{\rm max}$ of the dwarf. In the spheroidal stage, all the dispersions have similar values and they obey the relation $\sigma \sim V_{\rm max}/2$. They are also equal to the line-of-sight velocity dispersion measured for the galaxy (see Klimentowski et al. 2007). We also find that $V_{\rm max}$ traces reasonably well the total bound mass of the dwarf during the entire evolution. Assuming that the line-of-sight velocity dispersion can be reliably measured from kinematic data, the above facts suggest a new independent way of measuring the masses of dSphs.

These findings have intriguing implications for the missing satellites problem, which is normally formulated by measuring the number of subhaloes with a given value of $V_{\rm max}$. In particular, it suggests that circular velocities of observed dwarfs derived from either a simple isothermal halo model with a flat circular velocity profile (Moore et al. 1999) or line-of-sight velocity dispersions, assuming isotropic velocities (Klypin et al. 1999) were reasonable. This is true at least for dSphs that have a moderate mass-to-light ratio as our simulated dwarf (e.g. Fornax or Leo I). Dwarfs embedded in a much more massive dark matter halo may in principle have a different relation between σ and $V_{\rm max}$ since the stars could probe a region well inside the radius at which $V_{\rm max}$ occurs. Kazantzidis et al. (2004b) found that the stellar kinematics of Draco, that has $\sigma \sim 10 - 12$ km s^{-1}, can be reproduced in haloes with $V_{\rm max} \sim 25 - 30$ km s^{-1}, which would imply $\sigma/V_{\rm max} \sim 0.3 - 0.5$. A more recent study of Draco by Łokas, Mamon & Prada (2005), which took into account the contamination of the sample by tidal tails and included the fourth velocity moment in the analysis, found $\sigma \sim 8$ km s^{-1} and $V_{\rm max} \sim 16$ km s^{-1} again in agreement with the relation found here.

We find that the mass-to-light ratio of the dwarf drops significantly at the beginning of the evolution which is due to stripping of the extended dark halo. However, the ratio does not change significantly during the middle and late stages of the evolution. This suggests that very high values of dark matter content in some of the dSph galaxies, such as Draco or Ursa Major, are not an effect of tidal evolution but are rather the result of the formation process of their progenitors, or are caused by other mechanisms that affected their baryonic mass fraction. Photoevaporation of the gas after reionization (Babul & Rees 1992; Bullock, Kravtsov & Weinberg 2000; Barkana & Loeb 2001) could not cause the reduced baryon fraction. In fact our numerical experiment clearly shows that the original halo mass and $V_{\rm max}$ of a dSph produced by tidal stirring was significantly higher than it is today, and was well above the threshold below which photoevaporation is effective (this requires $V_{\rm max} < 15$ km s^{-1} according to the radiative transfer simulations of Susa & Umemura 2004). Instead, the combined effect of efficient heating by the cosmic ultraviolet background as the satellites fell into the MW halo at $z > 1$ and the ram pressure stripping in the gaseous corona around the MW disk might have removed most of the baryons, which remained in the gas phase rather than turning into stars (Mayer et al. 2007).

Recently Peñarrubia et al. (2008) studied tidal evolution of dSphs in a host potential assuming a King model for the stellar component. If the picture presented here is correct, then their assumption might not be very realistic, as in our case the dSph galaxy forms very late in the evolution. In particular, Peñarrubia et al. (2008) find that the result of the tidal evolution is to increase the mass-to-light ratio. This is due to the fact that the stars in their model are distributed according to the King profile with a core, so that

they are loosely bound and the stellar component is much more heavily stripped than in our case. In our simulation, the bar present for most of the time enhances the resilience of the stellar component to tidal stripping by increasing the depth of the potential well.

We have studied the internal kinematics of the dwarf and found that the velocity dispersions relax very quickly after the pericentre passages. This confirms that studies based on Jeans formalism (e.g. Łokas 2002; Łokas et al. 2005) should give reliable mass estimates for observed dSph galaxies. However, from the analysis of tidal tails we predict that in most cases the tails are aligned parallel to the line of sight of the observer who is placed inside the host galaxy. This suggests that many kinematic samples of dSph galaxies may be strongly contaminated by stars originating from the tails. This is something that needs to be taken into account when the goal is to model the masses of dwarfs (Łokas et al. 2005; Sánchez-Conde et al. 2007; Klimentowski et al. 2007).

Analysis of the tidal tails also shows that their density increases shortly after each pericentre passage and then drops with time. This density enhancement sometimes manifests itself as an abrupt 'tidal tail flipping', where old tails are destroyed and new ones are formed in a very short time. As a result one would expect that the number of stars contaminating the kinematic samples should be higher for dwarfs receding from the MW than for those approaching. We have also found an interesting linear relation between the velocity of stars in the tidal tails and their distance from the galaxy centre. Yet the slope of this relation changes during the evolution.

One potential problem which arises from our study is the fact that no bar-like structures are observed in the Local Group except for the Large Magellanic Cloud (LMC). It is not clear whether structures of this kind are detectable in such low surface brightness systems, but the simulation predicts that they should be quite common as this is likely to be the longest stage of the dwarf evolution. It is possible that at least several observed dSph galaxies could in reality be in a bar-like stage with the bar aligned along the line-of-sight and seen as spheroids due to projection effects. The LMC, which is known to have a more extended orbit than in the case of our simulated dwarf (Kallivayalil, van der Marel & Alcock 2006), consists of a bar and a thin stellar disk. Also, orbital evolution models using 3D velocities constrained by recent proper motion measurements suggest that the LMC may currently be on its first passage about the MW (Besla et al. 2007). The above confirm the picture we have presented, as we expect LMC to be less evolved and thus in some transitory stage between a stellar disk and a spheroid. However, most of the MW companions might indeed have had enough time to evolve into spheroidals since galaxy-sized haloes form early in CDM models and the MW halo was probably already in place at $z = 2$ (Governato et al. 2004, 2007). In addition, the present distances of most dSphs suggest that they were mostly accreted early (Mayer et al. 2007; Diemand et al. 2007). The situation is different in galaxy clusters which formed recently so the dwarfs did not have time to complete many orbits. Interestingly, many dwarfs in a transitional stage between a disky dwarf and a true dSph have been recently discovered in such environments (Lisker et al. 2007).

In this paper we have presented a self-consistent model for the evolution of a dwarf galaxy starting from the most natural progenitor expected in the CDM paradigm. This consists of a stellar disk embedded in a dark matter halo with the NFW profile. Cosmological simulations support the idea that isolated dwarfs are rotating disks, while pressure supported dwarfs are more abundant closer to the primary galaxy (Kravtsov et al. 2004a; Mayer 2005). We have shown how the evolution of such an object proceeds and how it is affected by the tidal forces of the host galaxy. The morphological evolution of a dwarf galaxy appears to be a dynamically rich process with several stages characterized by different events. In this picture recent high resolution simulations where a spheroidal object is postulated from the beginning (e.g. Peñarrubia et al. 2008; Muñoz et al. 2008) might not be adequate to describe how dSphs evolved under the action of the tidal field. In fact our results suggest that in most cases they could have transformed into spheroidal objects quite recently.

We argue that earlier attempts to model dSph galaxies as unbound and dark matter-free stellar remnants (Kroupa 1997) are ruled out based on our results. The tidal stirring model indeed demonstrates how tidal stripping and the formation of tidal tails naturally coexist with a substantial bound stellar component embedded in a relatively massive CDM halo even after several Gyr. Our results highlight the fact that tidal effects and the existence of a gravitationally bound dSph galaxy with a relatively high mass-to-light ratio are not mutually exclusive.

ACKNOWLEDGMENTS

We wish to thank S. Gottlöber and I. Shlosman for discussions. JK and EŁ are grateful for the hospitality of the Institut d'Astrophysique de Paris where part of this work was done. SK is funded by the Kavli Institute for Particle Astrophysics and Cosmology at Stanford University and the Center for Cosmology and Astro-Particle Physics at The Ohio State University. The numerical simulations were performed on the zBox1 supercomputer at the University of Zürich. This research was partially supported by the Polish Ministry of Science and Higher Education under grant N N203 0253 33 and the Jumelage program Astronomie France Pologne of CNRS/PAN.

REFERENCES

Athanassoula E., 2002, ApJ, 596, L83
Babul A., Rees M. J., 1992, MNRAS, 255, 346
Barkana R., Loeb A., 2001, Phys. Rep., 349, 125
Besla G., Kallivayalil N., Hernquist L., Robertson B., Cox T. J., van der Marel R. P., Alcock C., 2007, ApJ, 668, 949
Binney J., Tremaine S., 1987, Galactic Dynamics. Princeton Univ. Press, Princeton
Bullock J. S., Kravtsov A. V., Weinberg D. H., 2000, ApJ, 539, 517
Coleman M. G., Da Costa G. S., Bland-Hawthorn J., Freeman K. C., 2005, AJ, 129, 1443
Colpi M., Mayer L., Governato F., 1999, ApJ, 525, 720
Diemand J., Kuhlen M., Madau P., 2007, ApJ, 667, 859
Ghigna S., Moore B., Governato F., Lake G., Quinn T., Stadel J., 1998, MNRAS, 300, 146

Gilmore G., Wilkinson M. I., Wyse R. F. G., Kleyna J. T., Koch A., Evans W. N., Grebel E. K., 2007, ApJ, 663, 948
Governato F. et al., 2004, ApJ, 607, 688
Governato F., Willman B., Mayer L., Brooks A., Stinson G., Valenzuela O., Wadsley J., Quinn T., 2007, MNRAS, 374, 1479
Grebel E. K., Gallagher J. S., Harbeck D., 2003, AJ, 125, 1926
Hayashi E., Navarro J. F., Taylor J. E., Stadel J., Quinn T., 2003, ApJ, 584, 541
Helmi A., 2004, MNRAS, 351, 643
Johnston K. V., Sigurdsson S., Hernquist L., 1999, MNRAS, 302, 771
Kallivayalil N., van der Marel R. P., Alcock C., 2006, ApJ, 652, 1213
Kazantzidis S., Magorrian J., Moore B., 2004a, ApJ, 601, 37
Kazantzidis S., Mayer L., Mastropietro C., Diemand J., Stadel J., Moore B., 2004b, ApJ, 608, 663
Kazantzidis S., Kravtsov A. V., Zentner A. R., Allgood B., Nagai D., Moore B., 2004c, ApJ, 611, L73
Kleyna J. T., Wilkinson M. I., Evans N. W., Gilmore G., 2002, MNRAS, 330, 792
Klimentowski J., Łokas E. L., Kazantzidis S., Prada F., Mayer L., Mamon G. A., 2007, MNRAS, 378, 353
Klypin A., Kravtsov A. V., Valenzuela O., Prada F., 1999, ApJ, 522, 82
Klypin A., Kravtsov A. V., Bullock J. S., Primack J. R., 2001, ApJ, 554, 903
Kravtsov A. V., Berlind A. A., Wechsler R. H., Klypin A. A., Gottlöber S., Allgood B., Primack J. R., 2004b, ApJ, 609, 35
Kravtsov A. V., Gnedin O. Y., Klypin A. A., 2004a, ApJ, 609, 482
Kroupa P., 1997, NewA, 2, 139
Kuhn J. R., Miller R. H., 1989, ApJ, 341, 41
Lisker T., Grebel E. K., Binggeli B., Glatt K., 2007, ApJ, 660, 1186
Łokas E. L., 2001, MNRAS, 327, L21
Łokas E. L., 2002, MNRAS, 333, 697
Łokas E. L., Mamon G. A., Prada F., 2005, MNRAS, 363, 918
Martínez-Delgado D., Alonso-García J., Aparicio A., Gómez-Flechoso M. A., 2001, ApJ, 549, L63
Martinez-Vaquero L. A., Yepes G., Hoffman Y., 2007, MNRAS, 378, 1601
Mastropietro C., Moore B., Mayer L., Debattista V. P., Piffaretti R., Stadel J., 2005, MNRAS, 364, 607
Mateo M. L., 1998, ARA&A, 36, 435
Mayer L., 2005, in Jerjen H., Binggeli B., eds, Proc. IAU Coll. 198, Near-fields cosmology with dwarf elliptical galaxies. Cambridge Univ. Press, Cambridge, p. 220
Mayer L., Governato F., Colpi M., Moore B., Quinn T., Wadsley J., Stadel J., Lake G., 2001, ApJ, 559, 754
Mayer L., Kazantzidis S., Mastropietro C., Wadsley J., 2007, Nature, 445, 738
Milgrom M., 1995, ApJ, 455, 439
Montuori M., Capuzzo-Dolcetta R., Di Matteo P., Lepinette A., Miocchi P., 2007, ApJ, 659, 1212
Moore B., Ghigna S., Governato F., Lake G., Quinn T., Stadel J., Tozzi P., 1999, ApJ, L19
Muñoz R. R. et al., 2006, ApJ, 649, 201
Muñoz R. R., Majewski S. R., Johnston K. V., 2008, arXiv: 0712.4312v1
Peñarrubia J., McConnachie A. W., Navarro J. F., 2007, ApJ, 672, 904
Peñarrubia J., Navarro J. F., McConnachie A. W., 2008, ApJ, 673, 226
Piatek S., Pryor C., Bristow P., Olszewski E. W., Harris H. C., Mateo M., Minniti D., Tinney C. G., 2007, AJ, 133, 818
Sánchez-Conde M. A., Prada F., Łokas E. L., Gómez M. E., Wojtak R., Moles M., 2007, Phys. Rev. D, 76, 123509
Simon J. D., Geha M., 2007, ApJ, 670, 313
Sohn S. T. et al., 2007, ApJ, 663, 960
Stadel J. G., 2001, PhD thesis, Univ. of Washington
Strigari L. E., Koushiappas S. M., Bullock J. S., Kaplinghat M., 2007, Phys.Rev. D, 75, 83526
Susa H., Umemura M., 2004, ApJ, 610, L5
Taffoni G., Mayer L., Colpi M., Governato F., 2003, MNRAS, 341, 434
Taylor J. E., Babul A., 2001, ApJ, 559, 716
Walker M. G., Mateo M., Olszewski E. W., Bernstein R., Wang X., Woodroofe M., 2006, AJ, 131, 2114
Warnick K., Knebe A., 2006, MNRAS, 369, 1253